A Simple ML Detection for Coded Generalized Frequency Division Multiplexing in MIMO Channels

Mohammad Towliat, Seyyed Mohammad Javad Asgari Tabatabaee, and Morteza Rajabzadeh

***Abstract*—Generalized frequency division multiplexing (GFDM) is a promising multicarrier scheme, which has shown to be a good candidate to meet the rising demands of 5G networks. The inherent self-interference of GFDM prohibits the direct utilization of maximum likelihood (ML) detection of space-time coding (STC) in multi-input multi-output (MIMO) channels. Recently, a modified version of GFDM, called coded GFDM (CGFDM), has been proposed, which solves the problem of interference mitigation. In this paper, a simple near-optimal ML detection of Alamouti STC is proposed for MIMO CGFDM. Simulation results show that without sacrificing bandwidth efficiency, the proposed scheme outperforms the current MIMO GFDM detection techniques in terms of BER and computational complexity.**

***Index Terms*—GFDM, MIMO, ML detection, space-time coding.**

I. Introduction

In RECENT years, orthogonal frequency division multiplexing (OFDM) was the prevalent multicarrier system to combat the frequency selectivity of channels [1]–[3]. OFDM enjoyed its dominance due to simple implementation and adaptation to multi-input multi-output (MIMO) channels [4]. On the downside, OFDM suffers from some critical demerits which makes it to fall short to meet the rising demands of the next generation of communication networks [5]. Using rectangular pulse shapes in OFDM results in a high out of band (OOB) emission. Consequently, this system is not recommended for non-contiguous and fragmented band scenarios [6], [7]. It is shown that modified versions of OFDM, i.e., the filtered and windowed OFDM systems, provide a better performance in these scenarios [5]. Additionally, the cyclic prefix (CP), which is appended to each OFDM data frame, does not contain information-bearing data and degrades the bandwidth efficiency, particularly in highly dispersive channels [7], [8].

Amongst the alternative waveforms proposed to remedy the deficiencies of OFDM, generalized frequency division multiplexing (GFDM) is suggested as a suitable candidate to be used in the physical layer of the fifth generation (5G) networks [9]. GFDM is a block-wise system, in which a 2-dimensional block, containing the data symbols in time and frequency domains, is processed at both transmitter and receiver sides. In GFDM, OOB is reduced by using a well-localized pulse shape, instead of rectangular one [10]. The waveform design in this system is such that a CP is appended to each block of data symbols. Since, compared to OFDM frame, GFDM block potentially contains several times more data symbols, a considerable higher bandwidth efficiency can be provided in GFDM. The other remarkable point is that GFDM has larger number of samples per subchannel [11], which leads to a higher spectrum resolution and more accuracy in mitigating the effects of communication channel [10]. Besides, GFDM can adapt to MIMO channels to increase the performance and reliability which is one of the required demands in 5G networks [12].

Despite these advantageous features, the non-orthogonal nature of GFDM causes self-interference among the modulated data symbols in both time and frequency domains. Therefore, maximum likelihood (ML) detection of well-known spatial multiplexing (SM) [13] and space-time coding (STC) schemes cannot be directly deployed in MIMO GFDM [14]. Instead, the receiver needs to compensate the interference during the detection process. There are a wide range of non-optimal receivers for STC detection in MIMO GFDM. These receivers can be categorized in two main classes: non-iterative and iterative receivers. Obviously, non-iterative receivers generally are more complicated; whereas, they do not need any successive iterations to mitigate the interference [11], [15]–[17]. Contrarily, the main concern in iterative receivers is removing the interferences successively through several simple iterations [12], [18], [19].

Regarding the self-interference concerns, in [20] a modified GFDM scheme, titled as coded GFDM (CGFDM), is developed for single-input single-output (SISO) channels. In CGFDM a time reversal coding is employed to provide a unitary self-interference matrix, without degrading the bandwidth efficiency. In this paper we benefit from this feature of CGFDM to develop a simple near-optimal ML detection of Alamouti STC in MIMO CGFDM. We will show through simulations that the proposed ML detection scheme outperforms the standard STC detection techniques in MIMO GFDM in terms of both BER and computational complexity. The rest of this paper is organized as follows. In Section II, the GFDM background and its extension to MIMO channels is described. Section III contains the system model of CGFDM and the proposed ML detection of Alamouti STC in MIMO CGFDM. In Section IV we compare the complexity of the proposed method to that of standard detection techniques in MIMO GFDM. Simulation results are reported in Section V and, finally, Section VI concludes this paper.

Notations: Matrices are denoted by boldface uppercase letters (e.g., $\mathbf{A}$), vectors are indicated by letters with an upper arrow

Manuscript received May 2, 2018; revised August 27, 2018 and October 25, 2018; accepted November 12, 2018. Date of publication December 6, 2018; date of current version December 31, 2018. The associate editor coordinating the review of this manuscript and approving it for publication was Prof. Eleftherios Kofidis. *(Corresponding author: Seyyed Mohammad Javad Asgari Tabatabaee.)*

M. Towliat is with the Department of Electrical Engineering, Ferdowsi University of Mashhad, Mashhad 9177948974, Iran (e-mail: mohammad.toliat@mail.um.ac.ir).

S. M. J. Asgari Tabatabaee is with the Department of Electrical Engineering, University of Torbat Heydarieh, Torbat Heydarieh 9516168595, Iran (e-mail: s.m.j.asgaritabatabaee@torbath.ac.ir).

M. Rajabzadeh is with the Electrical Engineering Department, Quchan University of Technology, Quchan, Khorasan Razavi 9471784686, Iran (e-mail: m.rajabzadeh@qiet.ac.ir).

Digital Object Identifier 10.1109/TSP.2018.2885485

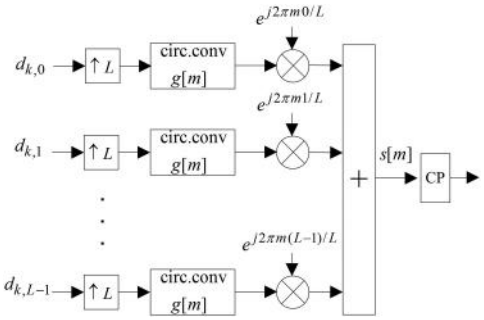

Fig. 1. GFDM transmitter.

(e.g., $\vec{A}$) and scalar quantities are presented by normal letters (e.g., A). $\mathbf{I}_N$ and $\mathbf{0}_N$ are the $N \times N$ identity and zero matrices, respectively. $|A|$ and $\|\mathbf{A}\|$ indicate the absolute value of scalar A and the Frobenius norm of matrix $\mathbf{A}$, respectively. Finally, the superscripts $(.)^T$, $(.)^H$ and $(.)^*$ indicate transpose, conjugate transpose and conjugate operators, respectively.

II. GFDM

A. System Model

GFDM is a block-wise multicarrier scheme, which modulates a block of data symbols in a given time-frequency lattice. Fig. 1 illustrates the GFDM transmitter, which is designed to transmit a data symbol block with length L subcarriers and width K subsymbols (i.e., $L \times K$ data symbol block). The output of the GFDM modulator is given as [10]

$$s[m] = \sum_{k=0}^{K-1} \sum_{l=0}^{L-1} d_{k,l} g_{k,l}[m]\,;\ \text{for } m = 0, \dots N-1, \qquad (1)$$

in which $N \triangleq LK$ and $d_{k,l}$ is the transmitted symbol at kth time instance and lth subchannel. Also, $g_{k,l}[m]$ is the time and frequency shifted version of the prototype filter $g[m]$, such that

$$g_{k,l}[m] \triangleq g[(m - kL)_N]\, e^{j2\pi ml/L}, \qquad (2)$$

where $(.)_N$ denotes the modulo of N. For the matrix-based representation, all transmitted symbols are stacked on top of each other in a single column vector as $\vec{d} \triangleq [\vec{d}_0^{\,T}, \dots \vec{d}_{K-1}^{\,T}]^T$, in which for $k = 0, \dots K-1$, $\vec{d}_k \triangleq [d_{k,0}, \dots d_{k,L-1}]^T$. Note that $\vec{d}$ and $\vec{d}_k$ are of the sizes $N \times 1$ and $L \times 1$, respectively. According to (1), the output vector of GFDM modulator for each data block, $\vec{s} \triangleq [s[0], \dots s[N-1]\ ]^T$, can be written as

$$\vec{s} = \mathbf{A}\vec{d}, \qquad (3)$$

in which $\mathbf{A}$, of the size $N \times N$, is the GFDM transmission matrix and is defined as

$$\mathbf{A} \triangleq [\mathbf{G}_0, \mathbf{G}_1, \dots \mathbf{G}_{K-1}], \qquad (4)$$

where, for $k = 0, \dots K-1$, $\mathbf{G}_k$ is an $N \times L$ matrix as follows

$$\mathbf{G}_k = \begin{bmatrix} g_{k,0}[0] & \cdots & g_{k,L-1}[0] \\ \vdots & \ddots & \vdots \\ g_{k,0}[N-1] & \cdots & g_{k,L-1}[N-1] \end{bmatrix}. \qquad (5)$$

According to Fig. 1, a CP is appended to $\vec{s}$, before it is transmitted through the channel. CP is a guard interval to avoid the collision between two consecutive modulated data symbol blocks passing the channel. The length of CP (i.e., ϑ) needs to be $\vartheta \geq L_{\mathrm{C}} - 1$, in which L_{C} is the length of the channel impulse response. At the receiver of GFDM, after removing CP, the received signal vector becomes [5]

$$\vec{y} = \mathbf{\Gamma}\vec{s} + \vec{w} = \mathbf{\Gamma}\mathbf{A}\vec{d} + \vec{w}, \qquad (6)$$

where $\vec{w}$ is the additive white Gaussian noise vector and $\mathbf{\Gamma}$ is the $N \times N$ circular matrix of the channel coefficients $h[m]$, for $m = 0, \dots L_{\mathrm{C}} - 1$.

B. Alamouti STC Detection in MIMO GFDM

Alamouti STC, which is introduced for 2 transmitter antennas, is the only orthogonal STC to achieve the full transmission diversity gain [21]. In this regard, in this section we consider the MIMO GFDM system with 2 transmitter and R receiver antennas and elaborate the standard receivers for Alamouti STC detection in MIMO GFDM and use them as our benchmark.

As explained in [10], at the first transmit antenna the data symbol vector $\vec{d}^{\,1}$ is modulated and, accordingly, $\vec{s}^{\,1} = \mathbf{A}\vec{d}^{\,1}$ is transmitted in the first time slot. Simultaneously, the second antenna modulates $\vec{d}^{\,2}$ with different data symbols and transmits $\vec{s}^{\,2} = \mathbf{A}\vec{d}^{\,2}$. In the next time slot, the first and second antennas transmit $-\vec{s}^{\,2*}$ and $\vec{s}^{\,1*}$, respectively. According to (6), the received signal vectors in both time slots are presented as

$$\begin{bmatrix} \vec{y}_1^{\,1} & \vec{y}_2^{\,1} \\ \vdots & \vdots \\ \vec{y}_1^{\,R} & \vec{y}_2^{\,R} \end{bmatrix} = \begin{bmatrix} \mathbf{\Gamma}^{1,1} & \mathbf{\Gamma}^{1,2} \\ \vdots & \vdots \\ \mathbf{\Gamma}^{R,1} & \mathbf{\Gamma}^{R,2} \end{bmatrix} \begin{bmatrix} \vec{s}^{\,1} & -\vec{s}^{\,2*} \\ \vec{s}^{\,2} & \vec{s}^{\,1*} \end{bmatrix} + \begin{bmatrix} \vec{w}_1^{\,1} & \vec{w}_2^{\,1} \\ \vdots & \vdots \\ \vec{w}_1^{\,R} & \vec{w}_2^{\,R} \end{bmatrix}, \qquad (7)$$

in which $\vec{y}_i^{\,r}$ and $\vec{w}_i^{\,r}$ (for $r = 1, ...R$ and $i = 1, 2$) are, respectively, the signal and noise at rth receiver and ith time slot. Also $\mathbf{\Gamma}^{r,t}$ (for $t = 1, 2$) is the circular channel matrix between rth receiver and tth transmitter. Regarding (7), Alamouti STC decoding is performed by estimating $\vec{s}^{\,1}$ and $\vec{s}^{\,2}$ as

$$\begin{aligned} \hat{\vec{s}}^{\,1} &= \left(\sum_{r=1}^{R} \mathbf{\Gamma}^{r,1}\mathbf{\Gamma}^{r,1*} + \mathbf{\Gamma}^{r,2}\mathbf{\Gamma}^{r,2*} \right)^{-1} \\ &\quad \left(\sum_{r=1}^{R} \mathbf{\Gamma}^{r,1*}\vec{y}_1^{\,r} + \mathbf{\Gamma}^{r,2}\vec{y}_2^{\,r\,*} \right) = \vec{s}^{\,1} + \vec{\varpi}^{\,1}, \\ \hat{\vec{s}}^{\,2} &= \left(\sum_{r=1}^{R} \mathbf{\Gamma}^{r,1}\mathbf{\Gamma}^{r,1*} + \mathbf{\Gamma}^{r,2}\mathbf{\Gamma}^{r,2*} \right)^{-1} \\ &\quad \left(\sum_{r=1}^{R} \mathbf{\Gamma}^{r,2*}\vec{y}_1^{\,r} - \mathbf{\Gamma}^{r,1}\vec{y}_2^{\,r\,*} \right) = \vec{s}^{\,2} + \vec{\varpi}^{\,2}, \end{aligned} \qquad (8)$$

where $\vec{\varpi}^1$ and $\vec{\varpi}^2$ are the resulted noises defined as

$$\vec{\varpi}^{\,1} = \left(\sum_{r=1}^{R} \mathbf{\Gamma}^{r,1}\mathbf{\Gamma}^{r,1*} + \mathbf{\Gamma}^{r,2}\mathbf{\Gamma}^{r,2*}\right)^{-1} \left(\sum_{r=1}^{R} \mathbf{\Gamma}^{r,1*}\vec{w}_1^{\,r} + \mathbf{\Gamma}^{r,2}\vec{w}_2^{\,r*}\right),$$
$$\vec{\varpi}^{\,2} = \left(\sum_{r=1}^{R} \mathbf{\Gamma}^{r,1}\mathbf{\Gamma}^{r,1*} + \mathbf{\Gamma}^{r,2}\mathbf{\Gamma}^{r,2*}\right)^{-1} \left(\sum_{r=1}^{R} \mathbf{\Gamma}^{r,2*}\vec{w}_1^{\,r} - \mathbf{\Gamma}^{r,1}\vec{w}_2^{\,r*}\right). \quad (9)$$

In (8), we can see that the MIMO GFDM stream has been transformed to two separate SISO GFDM streams. Moreover, estimations of $\vec{s}^{\,1}$ and $\vec{s}^{\,2}$ enjoy the full channel diversity gain. After that, the data symbol vectors can be detected by applying the SISO receiver matrix $\mathbf{Q}$ to the estimated signals, such that

$$\hat{\vec{d}}^{\,1} = \mathbf{Q}\hat{\vec{s}}^{\,1} = \mathbf{Q}(\mathbf{A}\vec{d}^{\,1} + \vec{\varpi}^{\,1}),$$
$$\hat{\vec{d}}^{\,2} = \mathbf{Q}\hat{\vec{s}}^{\,2} = \mathbf{Q}(\mathbf{A}\vec{d}^{\,2} + \vec{\varpi}^{\,2}). \quad (10)$$

There are three standard types of receivers to compensate the self-interference in SISO GFDM [10]: *i) Zero forcing (ZF) receiver*: in which $\mathbf{Q} = \mathbf{A}^{-1}$. Although the ZF receiver completely removes the self-interference, those small singular values of $\mathbf{A}$ lead to noise enhancement at $\hat{\vec{d}}^{\,1}$ and $\hat{\vec{d}}^{\,2}$ [22]. *ii) Matched filter (MF) receiver*: in which $\mathbf{Q} = \mathbf{A}^H$. In this case, there is no noise enhancement. However, because of non-orthogonality of $\mathbf{A}$ (i.e., $\mathbf{A}^H\mathbf{A} \neq \mathbf{I}_N$), the self-interference is not completely removed [20]. Thus, an extra successive interference canceller (SIC) is needed to remove the residual interference after MF. The resulted receiver is called MFSIC [23]. *iii) Minimum mean square error (MMSE) receiver*: where $\mathbf{Q} = \left(\mathbf{R}_{\varpi} + \mathbf{A}^H\mathbf{A}\right)^{-1}\mathbf{A}^H$ and $\mathbf{R}_{\varpi}$ is the covariance matrix of the noise vectors in (9). The MMSE receiver makes a compromise between noise enhancement and interference removal [10].

As discussed above, in MIMO GFDM, Alamouti coding is implemented on the output signals of GFDM modulators (i.e., $\vec{s}$), not on the input data symbols (i.e., $\vec{d}$). In this regard, at the receiver, the estimation of coded signals is performed by mitigating the channel effects, firstly (see (8)). At the next step, the data symbols are detected by eliminating the self-interference matrix from the estimated signals (see (10)). This two-leveled detection may increase the power of the final noise in (10) and, consequently, it leads to lower BER performance. To avoid this two-leveled noise enhancement, ML is suggested as the optimum detection method. Regarding (7), the ML detection of Alamouti STC in MIMO GFDM is given as [14]

$$[\hat{\vec{d}}^{\,1}\ \ \hat{\vec{d}}^{\,2}] = \underset{[\vec{d}^{\,1}\ \vec{d}^{\,2}]\in\Omega^U}{\arg\min}\ \|\mathbf{Y} - \mathbf{Z}\mathbf{S}\|^2, \quad (11)$$

in which

$$\mathbf{Y} \triangleq \begin{bmatrix} \vec{y}_1^{\,1} & \vec{y}_2^{\,1} \\ \vdots & \vdots \\ \vec{y}_1^{\,R} & \vec{y}_2^{\,R} \end{bmatrix}, \mathbf{Z} \triangleq \begin{bmatrix} \mathbf{\Gamma}^{1,1} & \mathbf{\Gamma}^{1,2} \\ \vdots & \vdots \\ \mathbf{\Gamma}^{R,1} & \mathbf{\Gamma}^{R,2} \end{bmatrix},$$
$$\mathbf{S} \triangleq \begin{bmatrix} \mathbf{A}\vec{d}^{\,1} & -(\mathbf{A}\vec{d}^{\,2})^* \\ \mathbf{A}\vec{d}^{\,2} & (\mathbf{A}\vec{d}^{\,1})^* \end{bmatrix}. \quad (12)$$

In (11), Ω is the modulation size, $U = 2N$ is the total number of STC coded data symbols in MIMO GFDM and Ω^U is the set of all possible states for $[\vec{d}^{\,1}\ \vec{d}^{\,2}]$. As it can be seen, in the procedure of ML detection, the channel effect and self-interference are considered all together and there is no enhancement on the noise. Unfortunately, because of the 3-dimensional interference (inter-symbol-interference, inter-channel-interference and inter-antenna-interference) among the data symbols, the ML detection (11) must be performed by seeking through all Ω^U possible states. This is a very complicated process and practically impossible [14]. Note that relations similar to (11) and (12) also hold for ML detection of Alamouti STC in MIMO OFDM, with the difference that $\mathbf{A}$ is replaced by the FFT matrix and because of diagonality of the channel matrix, the ML detection is performed separately for each individual data symbol. Consequently, the receiver's complexity becomes dramatically lower than that of MIMO GFDM.

Addressing these concerns about ML detection of Alamouti STC in MIMO GFDM, in the next section we elaborate the alternative CGFDM scheme (proposed in [20]) and then, develop a novel near-optimal and simple ML detection for Alamouti STC in MIMO CGFDM.

III. CGFDM

A. System Model

CGFDM employs a time reversal coding through a modified version of GFDM in SISO channels. The main advantage of CGFDM is that it provides a unitary self-interference matrix with the same bandwidth efficiency as the conventional GFDM. In this subsection we elaborate the CGFDM system model in SISO channel, which is slightly different from that explained in [20], but the main idea is the same.

Fig. 2 shows the transmitter of CGFDM. Obviously, CGFDM is the combination of two separate GFDM systems, one with the transmission matrix $\mathbf{A}$ (defined in (4)) and the other with the transmission matrix $\mathbf{B}$. Matrix $\mathbf{B}$ is similar to $\mathbf{A}$; with the exception that in $\mathbf{B}$ the prototype filter is $g[m - L/2]$ (while, in $\mathbf{A}$ it is $g[m]$). At the rest of this paper, in the structure of CGFDM, we mention the GFDM with the transmission matrix $\mathbf{A}$ as GFDM-A and the GFDM with the transmission matrix $\mathbf{B}$ as GFDM-B.

In CGFDM, data symbols are transmitted according to a two-stage time reversal coding. The data symbols at the second stage are the reformed version of the data symbols at the first stage. As a result, the bandwidth efficiency of CGFDM becomes equivalent to that of GFDM. Two transmission stages of CGFDM are as below:

1) Transmission at the First Stage: At the first stage, the independent data symbol vectors $\vec{d}$ and $\vec{d}\,'$, both with the size $N \times 1$, are modulated by GFDM-A and GFDM-B, respectively.

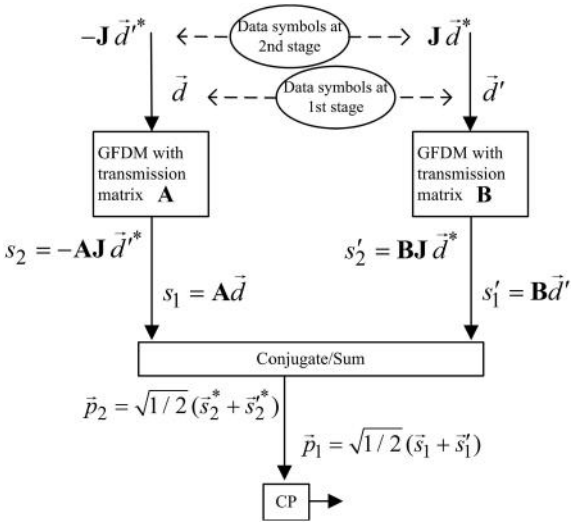

Fig. 2. CGFDM transmitter.

The outputs of modulators are given as

$$\begin{aligned} \vec{s}_1 &= \mathbf{A}\vec{d}, \\ \vec{s}_1' &= \mathbf{B}\vec{d}'. \end{aligned} \tag{13}$$

On the other hand, according to Fig. 2, the output of the CGFDM transmitter at the first stage is constructed as

$$\vec{p}_1 = \frac{1}{\sqrt{2}}\left(\vec{s}_1 + \vec{s}_1'\right) = \frac{1}{\sqrt{2}}\left[\mathbf{A} \quad \mathbf{B}\right]\begin{bmatrix}\vec{d} \\ \vec{d}'\end{bmatrix}, \tag{14}$$

In (14), factor $1/\sqrt{2}$ normalizes the power of outputs. Note that $\vec{p}_1$ is a column vector of the size $N \times 1$. Similar to Section II, a CP is appended to $\vec{p}_1$. At the receiver, after removing CP, the resulted signal becomes

$$\vec{x}_1 = \mathbf{\Gamma}\vec{p}_1 + \vec{w}_1 = \frac{1}{\sqrt{2}}\mathbf{\Gamma}\left[\mathbf{A} \quad \mathbf{B}\right]\begin{bmatrix}\vec{d} \\ \vec{d}'\end{bmatrix} + \vec{w}_1, \tag{15}$$

in which $\mathbf{\Gamma}$ is the circular channel matrix, exactly equivalent to that in (6), and $\vec{w}_1$ is the noise vector at the first stage.

2) Transmission at the Second Stage: At the second stage, the data symbol vectors $-\mathbf{J}\vec{d}^{*}$ and $\mathbf{J}\vec{d}^{*}$ are modulated by GFDM-A and GFDM-B, respectively. Thus, the outputs at this stage are obtained as

$$\begin{aligned} \vec{s}_2 &= -\mathbf{AJ}\vec{d}^{*}, \\ \vec{s}_2' &= \mathbf{BJ}\vec{d}^{*}, \end{aligned} \tag{16}$$

where $\mathbf{J}$ is an $N \times N$ unitary matrix defined as

$$\mathbf{J} \triangleq \underbrace{\begin{bmatrix} 1 & 0 & \cdots & 0 & 0 \\ 0 & 0 & \cdots & 0 & 1 \\ \vdots & 0 & 0 & 1 & 0 \\ \vdots & \iddots & \iddots & \iddots & 0 \\ 0 & 1 & 0 & 0 & 0 \end{bmatrix}}_{L\times L} \otimes \underbrace{\begin{bmatrix} 0 & 0 & \cdots & 0 & 1 \\ 0 & \cdots & 0 & 1 & 0 \\ \vdots & 0 & 1 & 0 & \vdots \\ 0 & \iddots & 0 & \vdots & 0 \\ 1 & 0 & \cdots & 0 & 0 \end{bmatrix}}_{K\times K}, \tag{17}$$

in which $\otimes$ denotes the Kronecker tensor product. For instance, Fig. 3 depicts matrix $\mathbf{J}$, when $L = 4$ and $K = 3$. Note that by multiplying $\mathbf{J}$ to a data symbol vector (in which data symbols of all subcarriers and subsymbols are stacked on top of each other), in the resulted vector, both time and frequency indices of data symbols are reversed, except the frequency index of 0th subcarrier.

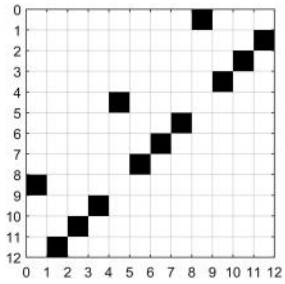

Fig. 3. Illustration of matrix $\mathbf{J}$, when $L = 4$ and $K = 3$. The black and white squares mean 1 and 0, respectively.

CGFDM modulator output at the second stage is given as

$$\vec{p}_2 = \frac{1}{\sqrt{2}}\left(\vec{s}_2^{*} + \vec{s}_2'^{*}\right) = \frac{1}{\sqrt{2}}\left[\mathbf{B}^{*}\mathbf{J} \quad -\mathbf{A}^{*}\mathbf{J}\right]\begin{bmatrix}\vec{d} \\ \vec{d}'\end{bmatrix}. \tag{18}$$

Similar to (15) at the receiver, we have

$$\vec{x}_2 = \mathbf{\Gamma}\vec{p}_2 + \vec{w}_2 = \frac{1}{\sqrt{2}}\mathbf{\Gamma}\left[\mathbf{B}^{*}\mathbf{J} \quad -\mathbf{A}^{*}\mathbf{J}\right]\begin{bmatrix}\vec{d} \\ \vec{d}'\end{bmatrix} + \vec{w}_2, \tag{19}$$

where $\vec{w}_2$ is the noise vector at the second stage.

At the end of these two stages, concatenation of (15) and (19) results in

$$\vec{X} = \mathbf{\Xi}\mathbf{\Lambda}\vec{D} + \vec{W}, \tag{20}$$

where $\vec{X} \triangleq [\vec{x}_1^{T} \quad \vec{x}_2^{T}]^{T}, \vec{D} \triangleq [\vec{d}^{T} \quad \vec{d}'^{T}]^{T}, \vec{W} \triangleq [\vec{w}_1^{T} \quad \vec{w}_2^{T}]^{T}$ and

$$\mathbf{\Xi} \triangleq \begin{bmatrix}\mathbf{\Gamma} & \mathbf{0}_N \\ \mathbf{0}_N & \mathbf{\Gamma}\end{bmatrix}, \quad \mathbf{\Lambda} \triangleq \frac{1}{\sqrt{2}}\begin{bmatrix}\mathbf{A} & \mathbf{B} \\ \mathbf{B}^{*}\mathbf{J} & -\mathbf{A}^{*}\mathbf{J}\end{bmatrix}. \tag{21}$$

According to (20), $\mathbf{\Lambda}$, of the size $2N \times 2N$, is the total self-interference matrix of CGFDM. The interesting property of $\mathbf{\Lambda}$ is its unitarity [20]. In other words, we have $\mathbf{\Lambda}^{H}\mathbf{\Lambda} = \mathbf{I}_{2N}$. In the next sections, we benefit the unitarity of the self-interference matrix to design a simple ML detection of Alamouti STC in MIMO CGFDM.

B. ML detection of Alamouti STC in MIMO CGFDM

As explained in Section II-B, in order to avoid the noise enhancements, ML can be a solution for detecting Alamouti STC in MIMO channels. However, in MIMO GFDM, the ML detection is associated with a huge complexity. To tackle this problem, in this section we propose a simple and near-optimal ML detection for Alamouti STC in MIMO CGFDM.

Consider a MIMO CGFDM which modulates data symbol vector $\vec{D}^{1}$ at the first antenna and data symbol vector $\vec{D}^{2}$ at the second antenna, simultaneously, in the first time slot (regarding (20) both $\vec{D}^{1}$ and $\vec{D}^{2}$ are vectors of the size $2N \times 1$). In the next time slot, the first antenna modulates $-\vec{D}^{2*}$ and the second antenna modulates $\vec{D}^{1*}$. According to (20), the received signals

can be written as

$$\begin{bmatrix} \vec{X}_1^1 & \vec{X}_2^1 \\ \vdots & \vdots \\ \vec{X}_1^R & \vec{X}_2^R \end{bmatrix} = \begin{bmatrix} \boldsymbol{\Xi}^{1,1} & \boldsymbol{\Xi}^{1,2} \\ \vdots & \vdots \\ \boldsymbol{\Xi}^{R,1} & \boldsymbol{\Xi}^{R,2} \end{bmatrix} \begin{bmatrix} \boldsymbol{\Lambda}\vec{D}^1 & -\boldsymbol{\Lambda}\vec{D}^{2*} \\ \boldsymbol{\Lambda}\vec{D}^2 & \boldsymbol{\Lambda}\vec{D}^{1*} \end{bmatrix} + \begin{bmatrix} \vec{W}_1^1 & \vec{W}_2^1 \\ \vdots & \vdots \\ \vec{W}_1^R & \vec{W}_2^R \end{bmatrix}, \tag{22}$$

in which $\vec{X}_i^r$ and $\vec{W}_i^r$ are, respectively, the received signal and noise at rth receiver and ith time slot. Also $\boldsymbol{\Xi}^{r,t}$ is the $2N \times 2N$ CGFDM channel matrix between rth receiver and tth transmitter. We can rewrite (22) as

$$\begin{bmatrix} \vec{X}_1^1 \\ \vdots \\ \vec{X}_1^R \\ \vec{X}_2^{1*} \\ \vdots \\ \vec{X}_2^{R*} \end{bmatrix} = \begin{bmatrix} \boldsymbol{\Xi}^{1,1}\boldsymbol{\Lambda} & \boldsymbol{\Xi}^{1,2}\boldsymbol{\Lambda} \\ \vdots & \vdots \\ \boldsymbol{\Xi}^{R,1}\boldsymbol{\Lambda} & \boldsymbol{\Xi}^{R,2}\boldsymbol{\Lambda} \\ (\boldsymbol{\Xi}^{1,2}\boldsymbol{\Lambda})^* & -(\boldsymbol{\Xi}^{1,1}\boldsymbol{\Lambda})^* \\ \vdots & \vdots \\ (\boldsymbol{\Xi}^{R,2}\boldsymbol{\Lambda})^* & -(\boldsymbol{\Xi}^{R,1}\boldsymbol{\Lambda})^* \end{bmatrix} \begin{bmatrix} \vec{D}^1 \\ \vec{D}^2 \end{bmatrix} + \begin{bmatrix} \vec{W}_1^{1\,T} & \cdots & \vec{W}_1^{R\,T} & \vec{W}_2^{1\,H} & \cdots & \vec{W}_2^{R\,H} \end{bmatrix}^T. \tag{23}$$

To derive our proposed ML detection method from (23), we use the following lemma.

Lemma 1: If the number of subchannels, L, is large enough, such that it can be assumed that the channel frequency response at each subchannel is flat over the spectrum of the prototype filter $g[m]$, then in the CGFDM system model (20), it can be approximated that

$$\boldsymbol{\Xi}\boldsymbol{\Lambda} \approx \boldsymbol{\Lambda}\mathbf{H}, \tag{24}$$

in which $\mathbf{H}$ is a $2N \times 2N$ diagonal matrix, defined as

$$\mathbf{H} = \underbrace{\begin{bmatrix} H[0] & & & \mathbf{0} \\ & H[1] & & \\ & & \ddots & \\ \mathbf{0} & & & H[L-1] \end{bmatrix}}_{L \times L} \otimes \mathbf{I}_{2K}, \tag{25}$$

where $H[l]$ (for $l = 0, ...L-1$) is the lth FFT component of the channel impulse response as $H[l] = \sum_{m=0}^{L_C-1} h[m]\, \exp(-j2\pi ml/L)$.

Proof: See Appendix A. ■

By using *lemma 1* and replacing $\boldsymbol{\Xi}\boldsymbol{\Lambda}$ with $\boldsymbol{\Lambda}\mathbf{H}$, (23) can be expressed as

$$\underbrace{\begin{bmatrix} \vec{X}_1^1 \\ \vdots \\ \vec{X}_1^R \\ \vec{X}_2^{1*} \\ \vdots \\ \vec{X}_2^{R*} \end{bmatrix}}_{\vec{\mathcal{X}}} \approx \underbrace{\begin{bmatrix} \boldsymbol{\Lambda}\mathbf{H}^{1,1} & \boldsymbol{\Lambda}\mathbf{H}^{1,2} \\ \vdots & \vdots \\ \boldsymbol{\Lambda}\mathbf{H}^{R,1} & \boldsymbol{\Lambda}\mathbf{H}^{R,2} \\ (\boldsymbol{\Lambda}\mathbf{H}^{1,2})^* & -(\boldsymbol{\Lambda}\mathbf{H}^{1,1})^* \\ \vdots & \vdots \\ (\boldsymbol{\Lambda}\mathbf{H}^{R,2})^* & -(\boldsymbol{\Lambda}\mathbf{H}^{R,1})^* \end{bmatrix}}_{\boldsymbol{\Theta}} \underbrace{\begin{bmatrix} \vec{D}^1 \\ \vec{D}^2 \end{bmatrix}}_{\vec{\mathcal{D}}} + \underbrace{\begin{bmatrix} \vec{W}_1^{1\,T} & \cdots & \vec{W}_1^{R\,T} & \vec{W}_2^{1\,H} & \cdots & \vec{W}_2^{R\,H} \end{bmatrix}^T}_{\vec{\mathcal{W}}}, \tag{26}$$

in which matrices $\mathbf{H}^{r,t}$ (for $r = 1, \ldots R$ and $t = 1, 2$) are diagonal. Now, let us define the MF matrix of MIMO CGFDM as

$$\mathbf{Q} \triangleq \begin{bmatrix} \boldsymbol{\Lambda}^H \otimes \mathbf{I}_R & \mathbf{0}_{2NR} \\ \mathbf{0}_{2NR} & \boldsymbol{\Lambda}^T \otimes \mathbf{I}_R \end{bmatrix}. \tag{27}$$

Because of unitarity of $\boldsymbol{\Lambda}$, $\mathbf{Q}$ is also a unitary matrix (i.e., $\mathbf{Q}^H\mathbf{Q} = \mathbf{I}_{4NR}$). Regarding (26), multiplying $\mathbf{Q}$ to $\vec{\mathcal{X}}$ leads to

$$\vec{\tilde{\mathcal{X}}} \approx \mathbf{Q}\boldsymbol{\Theta}\vec{\mathcal{D}} + \mathbf{Q}\vec{\mathcal{W}} = \tilde{\boldsymbol{\Theta}}\vec{\mathcal{D}} + \vec{\tilde{\mathcal{W}}}, \tag{28}$$

in which $\vec{\tilde{\mathcal{X}}} \triangleq \mathbf{Q}\vec{\mathcal{X}}$, $\tilde{\boldsymbol{\Theta}} \triangleq \mathbf{Q}\Theta$ and $\vec{\tilde{\mathcal{W}}} \triangleq \mathbf{Q}\vec{\mathcal{W}}$ is the resulted noise vector with the same covariance matrix as $\vec{\mathcal{W}}$ (because of unitarity of $\mathbf{Q}$). Note that according to the definition of $\mathbf{Q}$ and $\boldsymbol{\Theta}$, matrix $\tilde{\boldsymbol{\Theta}}$ becomes

$$\tilde{\boldsymbol{\Theta}} = \begin{bmatrix} \mathbf{H}^{1,1} & \mathbf{H}^{1,2} \\ \vdots & \vdots \\ \mathbf{H}^{R,1} & \mathbf{H}^{R,2} \\ \mathbf{H}^{1,2^*} & -\mathbf{H}^{1,1^*} \\ \vdots & \vdots \\ \mathbf{H}^{R,2^*} & -\mathbf{H}^{R,1^*} \end{bmatrix}, \tag{29}$$

in which each submatrix $\mathbf{H}^{r,t}$ is diagonal.

Considering (28), the ML detection of the data symbol vector $\vec{\mathcal{D}}$, of the size $4N \times 1$, is given as

$$\hat{\vec{\mathcal{D}}} = \underset{\vec{\mathcal{D}} \in \Omega^U}{\arg\min} \left\| \vec{\tilde{\mathcal{X}}} - \tilde{\boldsymbol{\Theta}}\vec{\mathcal{D}} \right\|^2, \tag{30}$$

where $U = 4N$ is the total number of STC coded data symbols in MIMO CGFDM. Since $\tilde{\boldsymbol{\Theta}}$ is with the structure of (29), it is concluded that $\tilde{\boldsymbol{\Theta}}^H\tilde{\boldsymbol{\Theta}}$ becomes diagonal. As a consequence, the ML detection of data symbol vector $\vec{\mathcal{D}}$ in (30) can be splitted up into separate ML detections for each individual data symbol. In other words, following the same procedure of ML detection in MIMO OFDM [24], it is easy to derive that (30) can be rewritten as

$$\hat{\mathcal{D}}_n = \underset{\mathcal{D}_n \in \Omega}{\arg\min} \left\| \vec{\tilde{\mathcal{X}}} - \vec{\tilde{\theta}}_n \mathcal{D}_n \right\|^2; \text{for } n = 0, \ldots 4N-1. \tag{31}$$

in which $\hat{\mathcal{D}}_n$ and $\mathcal{D}_n$ are respectively the nth entry of $\hat{\vec{\mathcal{D}}}$ and $\vec{\mathcal{D}}$. Also $\vec{\tilde{\theta}}_n$ denotes the nth column of $\tilde{\mathbf{\Theta}}$. Furthermore, according to (29), for nth column of $\tilde{\mathbf{\Theta}}$ we have $||\vec{\tilde{\theta}}_n||^2 = \sum_{r=1}^{R}\sum_{t=1}^{2}|H^{r,t}[(n)_L]|^2$, where $(.)_L$ denotes the modulo of L. This means that each ML detection in (31) enjoys the full MIMO channel diversity gain at the associated subchannel, which is similar to the ML detection of Alamouti STC in MIMO OFDM [25].

Eq. (31) presents the proposed ML detection of Alamouti STC in MIMO CGFDM, which does not cause any noise enhancements and can be performed with a very lower complexity compared to the detection methods in MIMO GFDM explained in Section II-B. However, because of the approximation in (24), the proposed detection method is near-optimal. Additionally, note that in Alamouti coding the channel is supposed to be time-invariant during the transmission of coded symbols in two time slots. Considering the fact that each time slot in CGFDM is twice as long as that of GFDM (compare (6) to (20)), it is deduced that the sensitivity of the proposed method to channel variations is more than that of MIMO GFDM receivers. In Section V, we numerically investigate this issue.

IV. Computational Complexity

In this section we elaborate the computational complexity of the proposed ML detection and the standard receivers of MIMO GFDM. To this end, we determine the number of complex multiplications (NCM) for each technique. Firstly, let us investigate the complexity of MIMO GFDM receivers. The channel removal in (8) contains $4RN^2 + 2N + N\log_2 N$ multiplications [26]. After that, discarding the self-interference in (10) by using ZF, MFSIC (proposed in [23]) and MMSE methods requires respectively $4N^2$, $2N(\log_2 N + \log_2 K + P + I(2\log_2 K + 1))$ and $\frac{2}{3}N^3 + 4N^2$ multiplications, where I is the number of iterations in MFSIC and P indicates the span of the prototype filter [26].

On the other hand, in the proposed ML detection for MIMO CGFDM, the MF procedure in (28) contains $8RN(2\log_2 N + \log_2 K + P)$ multiplications [26]. After that, in the detection process elaborated in (31), because of the structure of $\tilde{\mathbf{\Theta}}$, the calculation of Frobenius norm requires just $4R(N+1)+4N$ multiplications. Eventually, the total NCM for the proposed method is $8RN(2\log_2 N + \log_2 K + P) + 4R(N+1) + 4N$. Note that the determined NCM for ML detection in MIMO CGFDM is required for detecting $4N$ data symbols (see (31)), whereas the above presented NCM for MIMO GFDM receivers is for detecting just $2N$ data symbols (see (10)). In this regard, in order to compare the NCM of our proposed method to that of MIMO GFDM receivers, the total NCM of the proposed method must be considered with factor $\frac{1}{2}$. Table I summarizes the NCM of the mentioned methods, in case of detecting $2N$ data symbols. To have an intuitive interpretation of Table I, we numerically compare the NCM of these techniques in Section V.

TABLE I
Number of Complex Multiplications (NCM) in Various MIMO Receivers With R Antennas. The NCM Is Given for Detecting $2N$ Data Symbols

Technique	NCM
ZF in MIMO GFDM	$4RN^2 + 2N + N\log_2 N + 4N^2$
MFSIC in MIMO GFDM [23]	$4RN^2 + 2N + N\log_2 N + 2N(\log_2 N + \log_2 K + P + I(2\log_2 K + 1))$
MMSE in MIMO GFDM	$4RN^2 + 2N + N\log_2 N + \frac{2}{3}N^3 + 4N^2$
ML in MIMO CGFDM	$4RN(2\log_2 N + \log_2 K + P) + 2R(N+1) + 2N$

TABLE II
Parameters of Simulations

Parameter (General)	**Value/type**
Modulation	4-QAM
MIMO transmitters	2
MIMO receivers	$R = 2$
Sampling period	$t_s = 100$ ns
Carrier frequency	$f_c = 2$ GHz
Channel PDP	Vehicular-A, Pedestrian-B
CP length	$\vartheta = 40$
Channel coherence time	$T_C = \infty$, $90\,\mu$s
LDPC code word	576
LDPC rate	$5/6$
Parameter (GFDM and CGFDM)	**Value/type**
Number of subchannels	$L = 128$
Number of subsymbols	$K = 7$
Prototype filter	RRC ($\alpha = 0.5$), IOTA
Prototype filter span [23]	$P = 2$
Iterations in MFSIC [23]	$I = 8$
Parameter (OFDM)	**Value/type**
Block length	$LK = 896$

V. Simulation Results

In this section, we compare the performance of our proposed ML method of MIMO CGFDM to that of OFDM and MMSE GFDM,[1] when Alamouti STC is applied in MIMO channels. In our simulations we consider the MIMO channel with 2 transmitter and $R = 1$ and 2 receiver antennas. It is shown in [27] that GFDM can achieve a superior performance by using low density parity check (LDPC) code with soft decision. In this regard, in our simulations we consider that all systems are using soft-decision $5/6$ WiMAX LDPC coding with code word of 576 bits [28]. Note that in the ML detection (31), $\hat{\mathcal{D}}_n$ is a hard symbol and cannot be employed in soft-decision LDPC. In order to obtain soft symbols, since $||\vec{\tilde{\mathcal{X}}} - \vec{\tilde{\theta}}_n\hat{\mathcal{D}}_n||^2$ is convex with respect to $\hat{\mathcal{D}}_n$, it can be minimized by solving $\frac{\partial}{\partial\hat{\mathcal{D}}_n}||\vec{\tilde{\mathcal{X}}} - \vec{\tilde{\theta}}_n\hat{\mathcal{D}}_n||^2 = 0$. The solution of this equation is $\hat{\mathcal{D}}_n = (\vec{\tilde{\theta}}_n^H\vec{\tilde{\theta}}_n)^{-1}\vec{\tilde{\theta}}_n^H\vec{\tilde{\mathcal{X}}}$ [29]. Regarding that $\vec{\tilde{\theta}}_n$ is the nth column of $\tilde{\mathbf{\Theta}}$, replacing (29) and (25) in the solution leads us to

$$\hat{\mathcal{D}}_n = \frac{\sum_{r=1}^{R} H^{r,1*}[(n)_L]\tilde{\mathcal{X}}_{n+2N(r-1)} + H^{r,2}[(n)_L]\tilde{\mathcal{X}}_{n+2N(R+r-1)}}{\sum_{r=1}^{R}|H^{r,1}[(n)_L]|^2 + |H^{r,2}[(n)_L]|^2};$$
$$\text{for } n = 0,\dots 2N-1,$$
$$\hat{\mathcal{D}}_n = \frac{\sum_{r=1}^{R} H^{r,2*}[(n)_L]\tilde{\mathcal{X}}_{n+2N(r-2)} - H^{r,1}[(n)_L]\tilde{\mathcal{X}}_{n+2N(R+r-2)}}{\sum_{r=1}^{R}|H^{r,1}[(n)_L]|^2 + |H^{r,2}[(n)_L]|^2};$$
$$\text{for } n = 2N,\dots 4N-1. \quad (32)$$

[1] Among available receives for MIMO GFDM, the MMSE receiver has a good performance [20]. Thus, we just consider the performance of this receiver of MIMO GFDM, on behalf of other receivers.

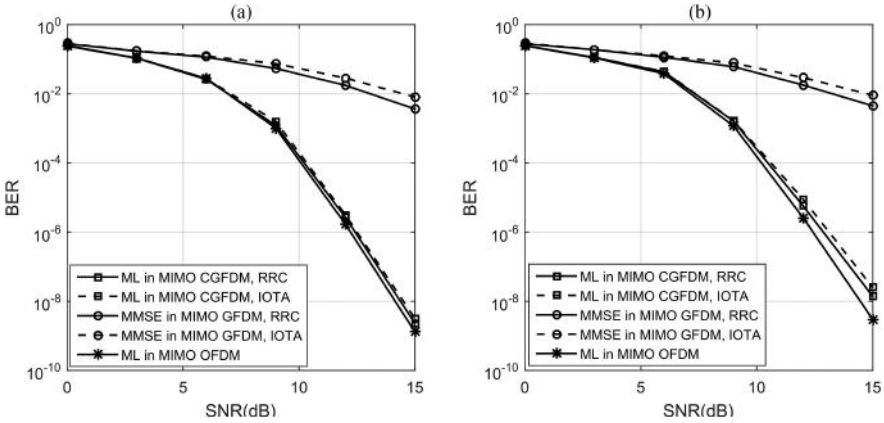

Fig. 4. The BER performance comparison for (a) time-invariant and (b) time-variant Vehicular-A 2×1 MIMO channel using RRC and IOTA prototype filters.

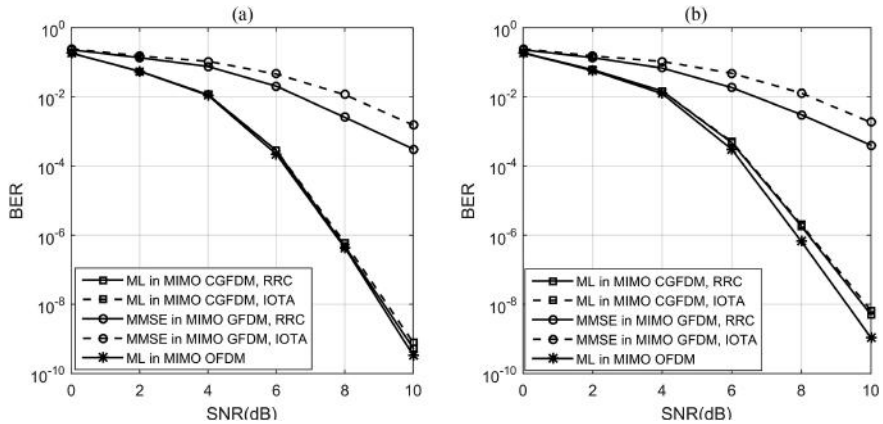

Fig. 5. The BER performance comparison for (a) time-invariant and (b) time-variant Vehicular-A 2×2 MIMO channel using RRC and IOTA prototype filters.

in which $\tilde{\mathcal{X}}_n$ is the nth entry of $\vec{\tilde{\mathcal{X}}}$. Now (32) provides a soft version of $\hat{\mathcal{D}}_n$ and can be utilized in soft-decision LDPC.

In addition, it must be noted that in GFDM when L and K are both even numbers, the self-interference matrix $\mathbf{A}$ becomes singular and the ZF and MMSE receivers are not applicable [22]. On the other hand, odd values of L or K impedes the simple implementation of GFDM. In this regard, in some works, such as [30] and [31], the authors design filters, for which even values of L and K do not result in a singular matrix $\mathbf{A}$. However, in CGFDM the self-interference matrix $\mathbf{\Lambda}$ is always unitary, regardless of the value of L and K. Nevertheless, in our simulations, we set L to an even number ($L = 128$) and K to an odd number ($K = 7$). The other simulation parameters are given in Table II.

In order to assess the accuracy of the approximation in *lemma 1*, we consider two prototype filters, including root raised cosine (RRC) and isotropic orthogonal transform algorithm (IOTA), introduced in [32]. Also, different power delay profiles (PDP) is considered for the frequency selective channel.

i) Vehicular-A channel model

The PDP of vehicular-A channel is [33]:

Delay = [0 300 700 1100 1700 2500] ns,

Power = [0 – 1 – 9 – 10 – 15 – 20] dB.

Fig. 4 compares the BER performances of all methods in 2×1 MIMO channel, when the channel coefficients are time-invariant (Fig. 4(a)) and time-variant (Fig. 4(b)) with the coherence time $T_{\mathrm{C}} = 90\mu$s. As it can be seen from Fig. 4(a), the performance of the proposed method is much better than that of MMSE in MIMO GFDM. Because the procedure of channel removal and then, self-interference mitigation leads to a dramatic noise enhancement in MIMO GFDM receivers. Instead, in the ML detection of MIMO CGFDM and MIMO OFDM no noise enhancement occurs. Additionally, it is clear that the BER of MMSE in MIMO GFDM, in case of IOTA filter, is higher than that of the RRC filter. These results show that in MMSE detection method, the IOTA filter causes more noise enhancement in self-interference cancellation than RRC. Moreover, the BER of the proposed method for both RRC and IOTA filters almost matches that of ML detection in MIMO OFDM, which shows that the approximation in (24) is accurate enough with these simulated parameters. In other words, with $L = 128$ subcarriers, the spectrum of both filters are narrow enough for which the Vehicular-A channel frequency response is flat over each subchannel. On the other hand, it can be seen in Fig. 4(b) that for time-variant channels, BER of all methods is higher than that in time-invariant channels. However, the channel variations affect CGFDM more than the other systems. We explained this drawback of the proposed method in Section III-B. Fig. 5, shows the BER performances for 2×2 MIMO channel. Compared to Fig. 4, all results are better, but still those of ML detection in MIMO CGFDM and MIMO OFDM are considerably superior.

ii) Pedestrian-B channel model

Now, let us repeat the simulations for Pedestrian-B channel model, where the time dispersion is longer than Vehicular-A. The PDP of Pedestrian-B is as follows [33]:

Delay = [0 200 800 1200 2300 3700] ns,

Power = [0 – 0.9 – 4.9 – 8 – 7.8 – 23.9] dB.

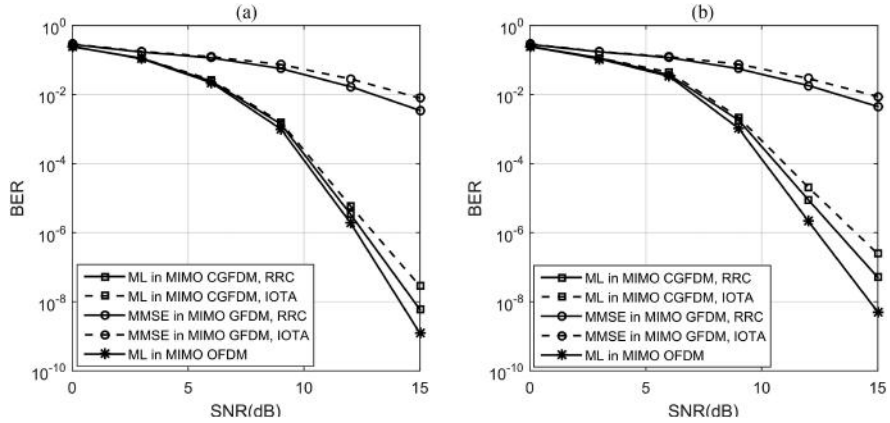

Fig. 6. The BER performance comparison for (a) time-invariant and (b) time-variant Pedestrian-B 2×1 MIMO channel using RRC and IOTA prototype filters.

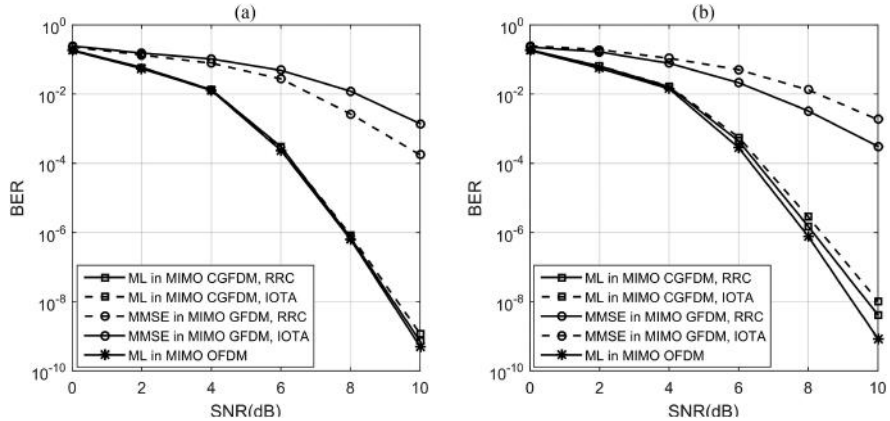

Fig. 7. The BER performance comparison for (a) time-invariant and (b) time-variant Pedestrian-B 2×2 MIMO channel using RRC and IOTA prototype filters.

In Fig. 6 we consider the 2×1 MIMO channel. Fig. 6(a) shows that, unlike Vehicular-A, the BER performance of the proposed ML detection in MIMO CGFDM does not match that of MIMO OFDM. The reason is that in such a frequency selective channel, the spectrum of channel cannot be assumed perfectly flat over each subchannel; as a result, the approximation in (24) is not accurate. The other remarkable point is that in Pedestrian-B channel, the RRC works better than IOTA in MIMO CGFDM, which means that RRC has a narrower spectrum than IOTA and results in a more accurate approximation in (24). In Fig. 6(b), compared to Fig. 6(a), all BER performances become worse, but that of the proposed method is more affected by channel time variations. These results confirm the more sensitivity of the proposed method to channel variations. Fig. 7 presents the simulation results when the MIMO channel is 2×2. Obviously, the performances are better than those in Fig. 6, but still the proposed method obtains a better result compared to MMSE receiver in MIMO GFDM.

To wrap it up, one can conclude from these simulations that in channels with smooth spectrum, the proposed ML method has a better performance compared to MIMO GFDM receivers. On the down side, the channel time variations affect the proposed method more than the other techniques. In channels with severe frequency selectivity, the less accurate approximation in the proposed method results in a higher BER. Using various prototype filters also can affect the performance. However, in all simulated scenarios above, the performance of our method is remarkably superior, compared to that of the MIMO GFDM receivers. Because we do not witness any noise enhancement in the proposed ML detection method.

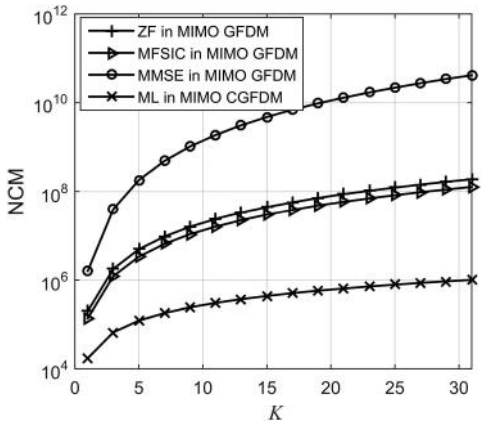

Fig. 8. Complexity of different techniques for Alamouti STC detection, when MIMO system has $R = 2$ receiver antennas.

Finally, Fig. 8 compares the complexity of the proposed ML detection to that of MIMO GFDM receivers in terms of NCM versus K, for $R = 2$ and $L = 128$. According to Fig. 8, it is obvious that NCM of the proposed method is dramatically lower than that of MIMO GFDM receivers. For example for $K = 7$

the NCM of the proposed ML detection is 1.804×10^5, while the NCM of ZF, MFSIC and MMSE receivers in MIMO GFDM is 6.554×10^6, 9.644×10^6 and 4.892×10^8. The supremacy of the proposed method, in terms of NCM, becomes more remarkable for larger values of K.

VI. Conclusion

Due to huge computational complexity, the ML detection of Alamouti STC is impracticable in MIMO GFDM system. On the other hand, removing interference by using standard receivers of MIMO GFDM (including ZF, MFSIC and MMSE) results in a two-leveled noise enhancement. Addressing these concerns, in this article we used the CGFDM system, as an alternative to GFDM. By considering the fact that the self-interference matrix in CGFDM is unitary, we developed a simple and near-optimal ML detection for Alamouti STC in MIMO CGFDM. The complexity of the proposed method is dramatically lower than that of standard MIMO GFDM receivers. Also, in terms of BER, the performance of our scheme is remarkably better.

Appendix A
Proof of Lemma 1

According to (21) we have

$$\mathbf{\Xi\Lambda} = \frac{1}{\sqrt{2}} \begin{bmatrix} \mathbf{\Gamma A} & \mathbf{\Gamma B} \\ \mathbf{\Gamma B}^* \mathbf{J} & -\mathbf{\Gamma A}^* \mathbf{J} \end{bmatrix}, \tag{33}$$

In the following, we elaborate each part of (33).

i) Evaluating $\mathbf{\Gamma A}$ and $\mathbf{\Gamma B}$:

In (33), let us first elaborate $\mathbf{\Gamma A}$. Considering the definition of $\mathbf{A}$ in (4), it can be derived that $\mathbf{\Gamma A} = [\mathbf{\Gamma G}_0, \mathbf{\Gamma G}_1, \dots \mathbf{\Gamma G}_{K-1}]$. If we define $\psi_{k,l}[m]$ as the (m,l)th entry of $\mathbf{\Gamma G}_k$, for $k = 0, \dots K-1$, then according to (5), it is obtained that

$$\begin{aligned} \psi_{k,l}[m] &= \sum_{a=0}^{N-1} h[a-m] g_{k,l}[a] \\ &= h[m] \overset{m}{\odot} g_{k,l}[m]; \quad \text{for } m = 0, \dots N-1. \end{aligned} \tag{34}$$

where $\overset{m}{\odot}$ denotes the circular convolution through index m with period N. By considering the definition of $g_{k,l}[m]$ in (2), taking N-point FFT from both sides of (34) leads to

$$\Psi_{k,l}[n] = \mathcal{H}[n] \mathcal{G}[n - lK]\, e^{-j2\pi k\, Ln/N}, \tag{35}$$

where $\Psi_{k,l}[n]$ and $\mathcal{G}[n]$ are the nth FFT components of $\psi_{k,l}[m]$ and $g[m]$, respectively. Also $\mathcal{H}[n] \triangleq \sum_{m=0}^{L_{\mathrm{C}}-1} h[m] \exp(-j2\pi mn/N)$ is the nth FFT component of $h[m]$. If the number of subchannels is large enough such that the channel spectrum (i.e., $\mathcal{H}[n]$) can be assumed flat over the prototype filter spectrum (i.e., $\mathcal{G}[n]$) at each subchannel, then (35) can be accurately approximated as [34]

$$\Psi_{k,l}[n] \approx \mathcal{H}[lK] \mathcal{G}[n - lK]\, e^{-j2\pi k\, Ln/N}. \tag{36}$$

According to the definition of $\mathcal{H}[n]$, it is derived that $\mathcal{H}[lK] = \sum_{m=0}^{L_{\mathrm{C}}-1} h[m] \exp(-j2\pi ml/L)$. In this regard, we can define $H[l] \triangleq \mathcal{H}[lK]$, where $H[l]$ is the lth component of L-point FFT of channel coefficients. Thus, (36) can be written as

$$\Psi_{k,l}[n] = H[l] \mathcal{G}[n - lK]\, e^{-j2\pi k\, Ln/N}. \tag{37}$$

Taking N-point IFFT from both sides of (37) leads to

$$\psi_{k,l}[m] \approx H[l] g_{k,l}[m]. \tag{38}$$

Since $\psi_{k,l}[m]$ is the (m,l)th entry of $\mathbf{\Gamma G}_k$, by using (38), it is concluded that

$$\mathbf{\Gamma G}_k \approx \mathbf{G}_k \underbrace{\begin{bmatrix} H[0] & & & \mathbf{0} \\ & H[1] & & \\ & & \ddots & \\ \mathbf{0} & & & H[L-1] \end{bmatrix}}_{\mathbf{E}}. \tag{39}$$

Besides, since $\mathbf{\Gamma A} = [\mathbf{\Gamma G}_0, \mathbf{\Gamma G}_1, \dots \mathbf{\Gamma G}_{K-1}]$ and (39) is derived for $k = 0, \dots K-1$, it is obtained that

$$\mathbf{\Gamma A} \approx \mathbf{A\Pi}, \tag{40}$$

where $\mathbf{\Pi} \triangleq \mathbf{E} \otimes \mathbf{I}_K$. In a similar way, it can be shown that in (33) for $\mathbf{\Gamma B}$ we have

$$\mathbf{\Gamma B} \approx \mathbf{B\Pi}, \tag{41}$$

ii) Evaluating $\mathbf{\Gamma A}^*$ and $\mathbf{\Gamma B}^*$:

Let us now evaluate $\mathbf{\Gamma A}^* = [\mathbf{\Gamma G}_0^*, \mathbf{\Gamma G}_1^*, \dots \mathbf{\Gamma G}_{K-1}^*]$. By defining $\varphi_{k,l}[m]$ as the (m,l)th entry of $\mathbf{\Gamma G}_k^*$, similar to (34), it is obtained that

$$\varphi_{k,l}[m] = h[m] \overset{m}{\odot} g_{k,l}^*[m]; \quad \text{for } m = 0, \dots N-1. \tag{42}$$

Taking N-point FFT from both sides of (42), it is concluded that

$$\Phi_{k,l}[n] = \mathcal{H}[n] \mathcal{G}[n - N + lK]\, e^{j2\pi k\, Ln/N}. \tag{43}$$

Following the same procedure of (36), (37) and (38), one can obtain that

$$\mathbf{\Gamma G}_k^* \approx \mathbf{G}_k^* \begin{bmatrix} H[0] & & & & \mathbf{0} \\ & H[L-1] & & & \\ & & H[L-2] & & \\ & & & \ddots & \\ \mathbf{0} & & & & H[1] \end{bmatrix}. \tag{44}$$

Since $\mathbf{\Gamma A}^* = [\mathbf{\Gamma G}_0^*, \mathbf{\Gamma G}_1^*, \dots \mathbf{\Gamma G}_{K-1}^*]$ and (44) is derived for $k = 0, \dots K-1$, finally, it is resulted that

$$\mathbf{\Gamma A}^* \approx \mathbf{A}^* \mathbf{J\Pi J}. \tag{45}$$

where $\mathbf{J}$ and $\mathbf{\Pi}$ are defined in (17) and (40), respectively. In a similar way, for $\mathbf{\Gamma B}^*$, it can be shown that

$$\mathbf{\Gamma B}^* \approx \mathbf{B}^* \mathbf{J\Pi J}. \tag{46}$$

Eventually, by substituting the achieved results in (40), (41), (45) and (46) into (33) and considering the fact that $\mathbf{J}$ is a unitary

matrix ($\mathbf{J}^H\mathbf{J} = \mathbf{J}\mathbf{J} = \mathbf{I}_N$), we have

$$\boldsymbol{\Xi}\boldsymbol{\Lambda} \approx \frac{1}{\sqrt{2}}\begin{bmatrix} \mathbf{A}\boldsymbol{\Pi} & \mathbf{B}\boldsymbol{\Pi} \\ \mathbf{B}^*\mathbf{J}\,\boldsymbol{\Pi} & -\mathbf{A}^*\mathbf{J}\,\boldsymbol{\Pi} \end{bmatrix} = \underbrace{\frac{1}{\sqrt{2}}\begin{bmatrix} \mathbf{A} & \mathbf{B} \\ \mathbf{B}^*\mathbf{J} & -\mathbf{A}^*\mathbf{J} \end{bmatrix}}_{\boldsymbol{\Lambda}} \underbrace{\begin{bmatrix} \boldsymbol{\Pi} & \mathbf{0}_N \\ \mathbf{0}_N & \boldsymbol{\Pi} \end{bmatrix}}_{\mathbf{H}} = \boldsymbol{\Lambda}\mathbf{H}. \quad (47)$$

Thus, it is concluded that $\boldsymbol{\Xi}\boldsymbol{\Lambda} \approx \boldsymbol{\Lambda}\mathbf{H}$, where, according to the definitions of $\boldsymbol{\Pi}$ in (40), $\mathbf{H}$ is a diagonal matrix given in (25).

REFERENCES

[1] R. v. Nee and R. Prasad, *OFDM for Wireless Multimedia Communications*. Norwood, MA, USA: Artech House, 2000.

[2] *IEEE Standard for Wireless LAN Medium Access Control (MAC) and Physical Layer (PHY) Specifications*, IEEE Standard 802.11-1997, pp. 1–445, Nov. 1997.

[3] *IEEE Standard for Air Interface for Broadband Wireless Access Systems*, IEEE Standard 802.16-2012 (Revision of IEEE Standard 802.16-2009), pp. 1–2542, Aug. 2012.

[4] I. Barhumi, G. Leus, and M. Moonen, "Optimal training design for MIMO OFDM systems in mobile wireless channels," *IEEE Trans. Signal Process.*, vol. 51, no. 6, pp. 1615–1624, Jun. 2003.

[5] B. Farhang-Boroujeny and H. Moradi, "OFDM inspired waveforms for 5G," *IEEE Commun. Surveys Tut.*, vol. 18, no. 4, pp. 2474–2492, Fourth Quarter 2016.

[6] G. Wunder *et al.*, "5GNOW: non-orthogonal, asynchronous waveforms for future mobile applications," *IEEE Commun. Mag.*, vol. 52, no. 2, pp. 97–105, Feb. 2014.

[7] M. Rajabzadeh and H. Steendam, "Power spectral analysis of UW-OFDM systems," *IEEE Trans. Commun.*, vol. 66, no. 6, pp. 2685–2695, Jun. 2018.

[8] S. M. J. Asgari Tabatabaee, M. Towliat, and F. S. Khodadad, "Joint equalization-despreading method for OQAM-CDMA systems," *Signal Process.*, vol. 146, pp. 92–98, 2018.

[9] G. Fettweis, M. Krondorf, and S. Bittner, "GFDM-generalized frequency division multiplexing," in *Proc. IEEE 69th Veh. Technol. Conf.*, 2009, pp. 1–4.

[10] N. Michailow *et al.*, "Generalized frequency division multiplexing for 5th generation cellular networks," *IEEE Trans. Commun.*, vol. 62, no. 9, pp. 3045–3061, Sep. 2014.

[11] M. Matthe, L. L. Mendes, N. Michailow, D. Zhang, and G. Fettweis, "Widely linear estimation for space-time-coded GFDM in low-latency applications," *IEEE Trans. Commun.*, vol. 63, no. 11, pp. 4501–4509, Nov. 2015.

[12] M. Matthe, D. Zhang, and G. Fettweis, "Iterative detection using MMSE-PIC demapping for MIMO-GFDM systems," in *Proc. 22nd Eur. Wireless Conf.*, 2016, pp. 1–7.

[13] H. Bolcskei, D. Gesbert, and A. J. Paulraj, "On the capacity of OFDM-based spatial multiplexing systems," *IEEE Trans. Commun.*, vol. 50, no. 2, pp. 225–234, Feb. 2002.

[14] M. Matthé, I. Gaspar, D. Zhang, and G. Fettweis, "Near-ML detection for MIMO-GFDM," in *Proc. IEEE 82nd Veh. Technol. Conf.*, 2015, pp. 1–2.

[15] M. Matthé, L. L. Mendes, and G. Fettweis, "Space-time coding for generalized frequency division multiplexing," in *Proc. 20th Eur. Wireless Conf.*, 2014, pp. 1–5.

[16] B. Picinbono and P. Chevalier, "Widely linear estimation with complex data," *IEEE Trans. Signal Process.*, vol. 43, pp. 2030–2033, Aug. 1995.

[17] M. Matthé, D. Zhang, and G. Fettweis, "Sphere-decoding aided SIC for MIMO-GFDM: Coded performance analysis," in *Proc. Int. Symp. Wireless Commun. Syst.*, 2016, pp. 165–169.

[18] D. Zhang, L. L. Mendes, M. Matthé, I. S. Gaspar, N. Michailow, and G. P. Fettweis, "Expectation propagation for near-optimum detection of MIMO-GFDM signals," *IEEE Trans. Wireless Commun.*, vol. 15, no. 2, pp. 1045–1062, Feb. 2016.

[19] D. Zhang, M. Matthé, L. L. Mendes, and G. Fettweis, "A Markov chain Monte Carlo algorithm for near-optimum detection of MIMO-GFDM signals," in *Proc. IEEE 26th Annu. Int. Symp. Pers., Indoor, Mobile Radio Commun.*, 2015, pp. 281–286.

[20] M. Towliat and S. M. J. A. Tabatabaee, "GFDM interference mitigation without noise enhancement," *IEEE Commun. Lett.*, vol. 22, no. 5, pp. 1042–1045, May 2018.

[21] S. M. Alamouti, "A simple transmit diversity technique for wireless communications," *IEEE J. Sel. Areas Commun.*, vol. 16, no. 8, pp. 1451–1458, Oct. 1998.

[22] M. Matthé, L. L. Mendes, and G. Fettweis, "Generalized frequency division multiplexing in a Gabor transform setting," *IEEE Commun. Lett.*, vol. 18, no. 8, pp. 1379–1382, Aug. 2014.

[23] I. Gaspar, N. Michailow, A. Navarro, E. Ohlmer, S. Krone, and G. Fettweis, "Low complexity GFDM receiver based on sparse frequency domain processing," in *Proc. IEEE 77th Veh. Technol. Conf.*, 2013, pp. 1–6.

[24] L. Hanzo, Y. Akhtman, J. Akhtman, L. Wang, and M. Jiang, *MIMO-OFDM for LTE, WiFi and WiMAX: Coherent Versus Non-Coherent and Cooperative Turbo Transceivers*. New York, NY, USA: Wiley, 2010.

[25] W. Zhang, X.-G. Xia, and K. B. Letaief, "Space-time/frequency coding for MIMO-OFDM in next generation broadband wireless systems," *IEEE Wireless Commun.*, vol. 14, no. 3, pp. 32–43, Jun. 2007.

[26] A. Farhang, N. Marchetti, and L. E. Doyle, "Low-complexity modem design for GFDM," *IEEE Trans. Signal Process.*, vol. 64, no. 6, pp. 1507–1518, Mar. 2016.

[27] M. Matthé, D. Zhang, and G. Fettweis, "Sphere-decoding aided SIC for MIMO-GFDM: Coded performance analysis," in *Proc. Int. Symp. Wireless Commun. Syst.*, 2016, pp. 165–169.

[28] *Air Interface for Fixed and Mobile Broadband Wireless Access Systems*, IEEE Standard 802.16e, Oct. 2005.

[29] G. A. Seber and A. J. Lee, *Linear Regression Analysis*, vol. 329. New York, NY, USA: Wiley, 2012.

[30] A. Nimr, M. Matthé, D. Zhang, and G. Fettweis, "Optimal radix-2 FFT compatible filters for GFDM," *IEEE Commun. Lett.*, vol. 21, no. 7, pp. 1497–1500, Jul. 2017.

[31] A. Yoshizawa, R. Kimura, and R. Sawai, "A singularity-free GFDM modulation scheme with parametric shaping filter sampling," in *Proc. IEEE 84th Veh. Technol. Conf.*, 2016, pp. 1–5.

[32] M. Alard, "Construction of a multicarrier signal," Patent WO, vol. 96, no. 35, p. 278, 1996.

[33] *Guidelines for Evaluation of Radio Transmission Technologies for IMT-2000*, ITU Recomm. M.1225, 1997.

[34] D. Katselis, E. Kofidis, A. Rontogiannis, and S. Theodoridis, "Preamble-based channel estimation for CP-OFDM and OFDM/OQAM systems: A comparative study," *IEEE Trans. Signal Process.*, vol. 58, no. 5, pp. 2911–2916, May 2010.

Mohammad Towliat received the B.Sc. degree in electrical engineering from Birjand University, Birjand, Iran, in 2009, and the M.S. degree in electrical engineering from the Ferdowsi University of Mashhad, Mashhad, Iran, in 2012. He is currently working toward the Ph.D. degree with the Department of Electrical and Computer Engineering, University of Delaware, Newark, DE, USA. His general interests include MIMO multicarrier systems and space-time coding techniques in communications.

Seyyed Mohammad Javad Asgari Tabatabaee received the B.Sc. and M.Sc. degrees in electrical engineering, the Ph.D. degree from the Ferdowsi University of Mashhad, Mashhad, Iran, in 2007, 2010, and 2016, respectively. He is an Assistant Professor with the Department of Electrical Engineering, University of Torbat Heydarieh, Torbat Heydarieh, Iran. His current research interests are multi-antenna techniques, optimization problems, and multicarrier modulations, especially FBMC and GFDM.

Morteza Rajabzadeh (M'14) received the B.Sc. (Hons.) and M.Sc. (Hons.) degrees in electrical engineering from Ferdowsi University, Mashhad, Iran, in 2005 and 2008, respectively, and the Ph.D. degree from the Ferdowsi University of Mashhad, Mashhad, Iran, in 2014. He is currently an Assistant Professor with the Quchan University of Technology, Quchan, Iran. His research interests include statistical signal processing, multicarrier techniques (especially CP-OFDM, GFDM, and UW-OFDM), and cognitive radio networks.